Available online at www.sciencedirect.com
SCIENCE DIRECT
Journal of Catalysis 229 (2005) 45–54
JOURNAL OF CATALYSIS
www.elsevier.com/locate/jcat

Coordination and oxidation changes undergone by iron species in Fe-MCM-22 upon template removal, activation and red–ox treatments: an in situ IR, EXAFS and XANES study

G. Berlier *, M. Pourny [1], S. Bordiga, G. Spoto, A. Zecchina, C. Lamberti *

Department of Inorganic, Physical and Materials Chemistry, University of Torino, via P. Giuria, 7 I-10125 Torino, Italy, and NIS Center of Excellence, University of Torino, Italy

Received 9 September 2004; revised 6 October 2004; accepted 8 October 2004

Abstract

We report about the characterization of an isomorphously substituted Fe-MCM-22 sample with high iron content (Si/Fe = 18) using FTIR, XANES and EXAFS spectroscopies. Template burning and subsequent activation in vacuo caused the migration of a fraction of framework Fe^{3+} species to extraframework positions, accompanied by the reduction of a fraction of Fe^{3+} to Fe^{2+}. A fraction of extraframework Fe^{2+} sites was able to adsorb NO, forming $Fe^{2+}(NO)_n$ complexes ($n = 1, 2, 3$), which indicates a high coordinative unsaturation of such sites. The parallel experiment monitored by X-ray absorption spectroscopies testified that this fraction is however small, as both EXAFS and XANES spectra were almost unperturbed by NO adsorption. The corresponding FTIR bands are highly broad and asymmetric, which does not allow to detect the presence of $Fe^{3+}(NO)$ complexes. The broad character of the nitrosyl bands suggests the presence of small oxidic clusters, in agreement with XANES and EXAFS evidences. The nature and distribution of extraframework Fe species are influenced by water preadsorption, which causes the increase of the amount of the most coordinatively unsaturated Fe^{2+} sites, able to form $Fe^{2+}(NO)_3$ complexes. The effect of red–ox treatments with O_2 and H_2 was also investigated. Upon oxidation, adsorbed oxygen is formed, which efficiently shields the Fe centers and does not rapidly nor efficiently react with NO. Upon reduction, the intensity of nitrosyl complexes increases, indicating the reduction of extraframework Fe^{3+} (likely present on the surface of small oxidic clusters) to Fe^{2+}. Comparison with the most investigated Fe-MFI system is made.

Keywords: Fe-zeolite; MCM-22; Benzene hydroxylation; IR; NO; EXAFS; XANES

1. Introduction

Insertion of trivalent heteroatoms, like Al [1], Ga [2], or Fe [3–5] into T positions in the crystalline framework of zeolites is accompanied by the appearance of strong Brønsted acidity (bridged T(OH)Si sites), responsible for the acidic catalytic activity of these materials. The stability of Al atoms in T position is much higher than that of Ga or Fe [5,6]. As a consequence, thermal treatments cause the migration of Ga or Fe to extraframework positions and their progressive aggregation in form of isolated, dimeric and polymeric species up to oxidic nanoparticles [4,5,7,8]. This migration leads to the appearance of a different type of acid sites of Lewis nature [4,5,9,10]. As a consequence, after this treatment Fe-zeolites can possess both Brønsted and Lewis acid sites, working separately or in a synergistic way in acid-catalyzed reactions [11–13].

Extraframework iron cations can show different valence states (Fe^{2+}, Fe^{3+} and even Fe^{4+}) depending upon the reducing or oxidising character of the reagents present in the catalyst environment and hence show red–ox properties not available in Al- or Ga-silicalites. An important example of

* Corresponding authors. Fax: +39011-6707855.
E-mail addresses: gloria.berlier@unito.it (G. Berlier), carlo.lamberti@unito.it (C. Lamberti).
[1] Present address: Silicon Chemistry Research Group, Department of Chemistry, Open University, Walton Hall, Milton Keynes, MK7 6AA, UK.

0021-9517/$ – see front matter
doi:10.1016/j.jcat.2004.10.007

catalytic activity associated with this interplay between different oxidation states of Fe, hosted in the MFI framework, is the partial oxidation of benzene to phenol using N_2O as oxidising agent [14,15]. The selective insertion of the hydroxyl group into the aromatic ring to yield phenols, naphthols and so on, is a very promising tool for the chemical industry, the commonly employed route via the three-step cumene process being of great complexity [16]. Besides the benzene to phenol reaction, iron containing zeolites have shown promising results in the de-NO_x catalysis [17–21]. Due to the high industrial interest related to this topic, a remarkable number of scientific works have appeared concerning iron containing zeolitic systems. Two different main preparation procedures have been employed till now to disperse iron species inside the zeolite channels: (i) post-synthesis insertion via ion exchange [17–27], and (ii) isomorphous insertion of Fe^{3+} into the MFI framework during the zeolite synthesis [4–8,28–36].

Most of the before mentioned bibliography refers to iron species introduced inside the MFI matrix. However, as far as the isomorphous substitution method is concerned, very low percentage of iron can be incorporated. Besides MFI, other iron containing zeolitic frameworks like mordenite, beta, ferrierite and mesoporous silicas have been investigated for the reactions outlined before [20,37–42]. Among them also MCM-22 [43,44] (MWW framework) has been used as hosting material for Fe isomorphous substitution [39–42]. This material is particularly interesting as a considerably higher amount of iron can be introduced in the T sites of its framework.

From a structural point of view MCM-22 is characterised by a complex porosity, containing both medium and large pores [43,45–47]. The structural complexity derives from the presence of two independent pore systems accessible through 10-ring openings. One of these systems is defined by two-dimensional sinusoidal channels, maintaining an effective 10-ring diameter throughout the structure. The second one includes large supercages with 12-ring openings defined by inner diameter of 7.1 Å and inner length of 18.2 Å.

This work is devoted to the study of a Fe-MCM-22 sample with a high concentration of Fe (Si/Fe = 18) prepared by isomorphous insertion. We will follow the effect of template burning in air and of the subsequent activation in vacuo at 773 K on (i) the migration of Fe species from the T position, (ii) the heterogeneity, and (iii) the oxidation state of the extraframework species. Finally, the effect of interaction with water, and of red–ox treatments (with H_2 or O_2), has been investigated. The main characterisation techniques have been IR spectroscopy of adsorbed NO, supported by parallel EXAFS and XANES studies. This choice has been adopted on the basis of literature data, that have shown both IR [5,7,34–36,38,39,48–50] and X-ray absorption [4–6,8,32,33,51–54] spectroscopies as the most informative techniques in the characterisation of Fe in zeolites.

2. Experimental and methods

The Fe-MCM-22 (Si/Fe = 18 and Si/Al = 90) catalyst was prepared by the Aiello group (University of Calabria, I) following the method described in detail in Ref. [41]. The sample was calcined in dry air flow of 10 $cm^3\,min^{-1}$ at 873 K for 6 h. The sample in presence of template has been characterised by EXAFS and XANES techniques only. EXAFS, XANES, and IR spectroscopies have been used to study the calcined sample subsequently activated at 773 K in vacuo. Oxidation (reduction) treatments were performed in O_2 (H_2) atmosphere at 573 K and were investigated by means of IR spectroscopy only. Water dosage at RT has also been studied to investigate its effect on the nuclearity of extraframework iron clusters.

X-ray absorption experiments were performed at the GILDA MB8 beamline [55] at the European Synchrotron Radiation Facility (ESRF). The monochromator was equipped with two Si(311) crystals and harmonic rejection was achieved using mirrors. In order to assure high quality XANES spectra, the geometry of the beamline was optimized to improve the energy resolution: vertical slits, located at 23 m from the source, were set to 0.6 mm assuring at 7 KeV, an actual energy resolution better than 0.4 eV. The following experimental geometry was adopted: 1) I_0 (1 bar N_2 filled ionization detector having efficiency of 10%); 2) zeolite sample; 3) I_1 (100 mbar Ar filled ionization detector having efficiency of 50%); 4) 3 μm thick iron metal foil; 5) I_2 (photodetector). This set-up allows a direct energy/angle calibration for each spectrum avoiding any problem related to minor energy shifts due to small thermal instability of the monochromator crystals [56]. A sampling step of 0.2 eV for the XANES part of the spectra and a variable sampling step, giving $\Delta k_{max} = 0.05$ $Å^{-1}$ for the EXAFS part, and an integration time of 3 s/point have been adopted. Spectra were collected at room temperature (RT) using a metallic cell allowing in situ high temperature treatments and gas dosage [57]. A more complete description on both experimental set-up and EXAFS data analysis is reported in Ref. [8], devoted to the characterisation of the parent Fe-silicalite system.

The IR experiments were carried out on a Bruker IFS 66 FTIR instrument equipped with a cryogenic MCT detector and running at 2 cm^{-1} resolution. The samples were in the form of self-supporting pellets suitable for measurements in transmission mode. Measurement cells were used allowing in situ thermal and oxidative treatments. NO, carefully purified by distillation in order to remove other undesired nitrogen oxides, was initially dosed at RT, at an equilibrium pressure (P_{NO}) of 15 Torr. After 1 h the equilibrium pressure was reduced step by step, so allowing to obtain a sequence of IR spectra corresponding to decreasing NO coverage [5]. The last spectrum typically corresponded to 15 min outgassing at RT (residual pressure lower than 10^{-3} Torr). The IR spectrum collected before gas dosage was used as background

for obtaining the background-subtracted spectra reported in the following.

3. Results and discussion

3.1. EXAFS

The three curves of Fig. 1a report the $k\chi(k)$ function of the Fe-MCM-22 sample in the presence of template (full line curve), after template removal and subsequent activation at 773 K (dashed curve) and after subsequent interaction with NO (dotted curve, hardly distinguishable from the activated one). Just a superficial view on the experimental data finds a significant decrease of the EXAFS signal upon activation at 773 K. In fact, while the spectrum collected in the presence of the template shows up to six complete oscillations, the last maximum being appreciable on this view around 13.0 $Å^{-1}$, only four periods are observed above the noise level, for the sample activated at 773 K, being the last appreciable maximum at approximately 9.0 $Å^{-1}$. The remarkable decrease of the EXAFS signal is also reflected in the corresponding k^3-weighted, phase uncorrected, FT reported in Fig. 1b, where the intensity of the Fe–O first shell peak falls down from 9.7 to 4.3 $Å^{-4}$.

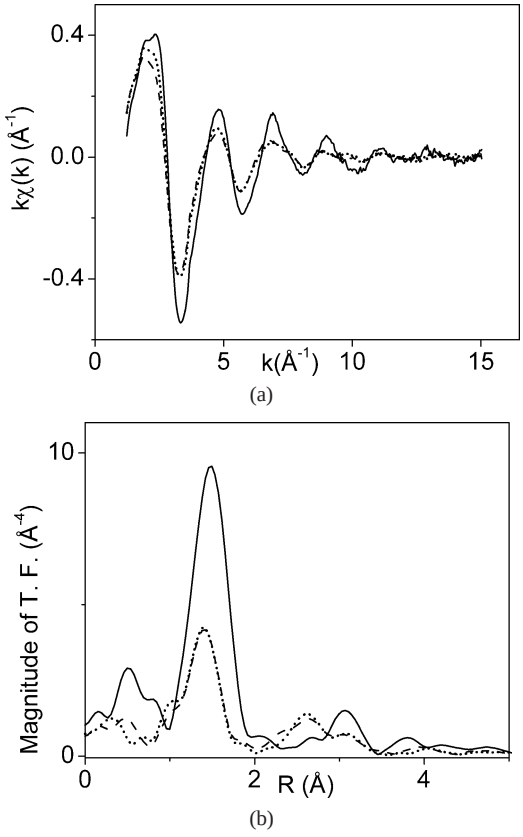

Fig. 1. (a) Experimental $k\chi(k)$ of the Fe-MCM-22 sample in the presence of template (full line), after removing template and subsequent activation at 773 K (dashed line), and after subsequent interaction with 15 Torr of NO at RT (dotted line); (b) Corresponding k^3-weighted, phase uncorrected FTs.

The three pairs of superimposed curves reported in Fig. 2 concern the comparison between the first shell filtered $k\chi(k)$ function and its best fit modeled as a single Fe–O contribution for the Fe-MCM-22 sample measured with template, after activation at 773 K and subsequent interaction with NO (first, second and third from top, respectively). The results of these fits are summarized in Table 1. As far as the sample containing the template is concerned, a coordination number of 4 (within the experimental error) is measured, with an average distance Fe–O of 1.87 ± 0.01 Å. This corresponds to the presence of isolated Fe species inside the zeolitic framework in tetrahedral coordination. Note that similar Fe–O distances were observed for Fe introduced in different zeolitic networks, such as Fe-silicalite and Fe-ZSM-5 samples [4–6,8,32,33].

The reduction of the average coordination number measured on the sample after activation at 773 K (Table 1) is a direct consequence of the decrease of the EXAFS signal (Fig. 1a). A similar phenomenon (even more dramatic) was observed upon activation of Fe-silicalite [4,5,8] and was explained by the formation of a complex distribution of extraframework Fe species characterised by a high heterogeneity of local environments. In fact, when Fe atoms occupy tetrahedral framework positions, they have a well defined

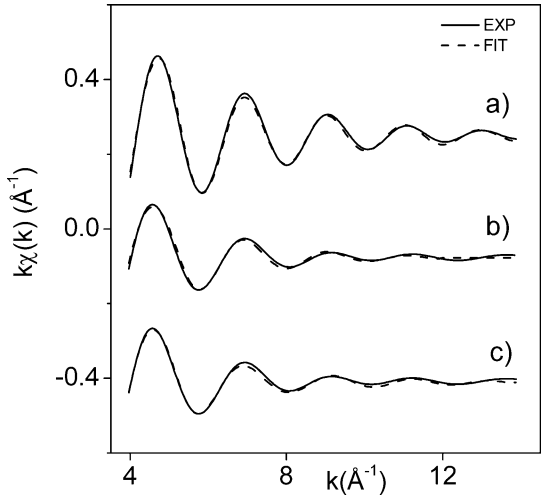

Fig. 2. Fourier filtered $k\chi(k)$ functions (full lines) and corresponding best fits performed using a single Fe–O contribution as model (dashed lines). From top to bottom: a) sample with template, b) after removing template and subsequent activation at 773 K, and c) after subsequent interaction with 15 Torr of NO at RT. Curves where vertically shifted for clarity.

Table 1
Results of the EXAFS data analysis for the catalyst measured in different conditions: iron coordination number (N), Fe–O bond length (R), Debye–Waller parameter (σ), and energy shift of the Fe K-edge (ΔE)

Sample condition	N	R (Å)	σ (Å)	ΔE (eV)
With template	3.8 ± 0.4	1.87 ± 0.01	$(5 \pm 1) \times 10^{-2}$	7 ± 2
Activated at 773 K	2.8 ± 0.3	1.86 ± 0.02	$(9 \pm 1) \times 10^{-2}$	3 ± 2
Activated at 773 K + NO	2.7 ± 0.3	1.85 ± 0.03	$(9 \pm 2) \times 10^{-2}$	3 ± 2

and ordered first shell environment, characterised by 4 oxygen ligands at a well defined Fe–O distance (1.87 ± 0.01 Å). This ordered situation gives rise to a constructive accumulation of the EXAFS signal coming from the different absorbing iron sites, yielding (within experimental errors) a Fe–O coordination number of 4 (see Table 1). When a fraction of iron atoms migrates into extraframework positions, as often observed in Fe-MFI systems [4,5,8], a mixture of Fe species characterized by different oxidation, coordination and aggregation states (from isolated species to small oxidic clusters) is formed. Such heterogeneity implies that the local environment of Fe atoms has a continuous spread in Fe–O bond distances, dynamic Debye–Waller factors and coordination numbers (please note that by O we mean oxygen atoms of both oxidic nanocluster and zeolitic framework anchoring sites). From what we have learnt from the Fe-silicalite case, the EXAFS signal coming from extraframework iron species is affected by such a large Debye–Waller factor (of static origin) as to become practically undetectable [5,8,35,58] for $k > 5$ Å^{-1}, where the observed EXAFS oscillations are mainly due to the complementary fraction of Fe atoms still occupying framework positions. Since all iron atoms contribute to the edge jump in the measured μx spectrum, and since the reported $\chi(k)$ functions are normalized to this jump, the dramatic decrease of the EXAFS signal is thus qualitatively explained. According to this interpretation, the fraction of framework Fe species in the activated sample is evaluated as N/4. Of course, this model gives an overestimated fraction value because the complete elimination of the EXAFS oscillations holds only in the high k region, while at low k the phase difference between different Fe–O contributions is not resulting in a completely destructive interference.

In our case this model gives a value of 0.70 ± 0.08. This value is much higher than that observed for Fe-silicalite activated in the same conditions (0.42 ± 0.08) [8]. This impressive difference reflects the greater ability of the MCM-22 framework in hosting trivalent heteroatoms as: (i) low Si/Al ratio can be reached and (ii) low tendency to de-alumination process has been reported [42,59].

The apparent shortening of the Fe–O bond length in the samples treated at 773 K (also observed for Fe-silicalite samples [5,8]) and after interaction with NO (Table 1) can also be explained in terms of structural disorder of extraframework iron species. The effect of a large disorder is equivalent to a system having an asymmetrical radial distribution function, which can lead to an apparent contraction of bond length in the usual analysis of EXAFS data [60,61]. Although the observed Fe–O bond length shortening lies within the experimental errors (Table 1), this trend seems to have a general validity as already observed during extraframework migration processes in both Fe-silicalite [5,8] and Ga-silicalite [62] systems. The average Fe–O distances measured by EXAFS on the activated samples deserve additional comment. When iron is introduced in the zeolite pores via post-synthesis methods (e.g. by $FeCl_3$ sublimation), significantly longer Fe–O distances (from 1.96 to 2.13 Å) are observed [23,52–54]. The absence of any evident elongation of the Fe–O bond distance upon sample activation represents a further proof of the thesis that, in the present case, extraframework Fe species result in insignificant contribution to the overall EXAFS signal.

Finally, the EXAFS signal is not sensibly affected by the interaction of NO with the activated sample (Fig. 1, compare dashed and dotted curves). This evidence is in apparent contradiction to the IR experiments which show that NO is strongly interacting with extraframework Fe^{2+} species forming stable nitrosyl complexes (vide infra). However, it is important to underline the fact that nitrosyl complexes are formed on the fraction of extraframework Fe^{2+} species, that is, the EXAFS silent fraction.

3.2. XANES

XANES spectroscopy is one of the most informative techniques for the determination of oxidation states and of local symmetries of transition metal ions [56,57,63–65]. This is particularly true when appropriate model compounds, with well defined oxidation and coordination states, are available for comparison [4,5,8,63,65,66]. In the present case we have measured $FePO_4$, as an example of Fe^{3+} in tetrahedral coordination, $Fe(acac)_3$ and α-Fe_2O_3 for Fe^{3+} in octahedral symmetry. $FeCp_2$ has been chosen as an example of a Fe^{2+} compound (acac = acetylacetonate, Cp = cyclopentadienyl). The XANES spectra of these model compounds have been reported and discussed extensively in Ref. [5]. For the sake of comparison, both position and intensity of the $1s \rightarrow 3d$ pre-edge peaks have been summarized in Table 2.

The most evident change in the XANES spectra reported in Fig. 3 concerns the red shift of about 1.0 eV of the absorption edge upon calcination and subsequent thermal activation in vacuo. A greater shift, of 1.2 and 3.0 eV has been observed after activation of Fe-silicalite samples at 773 and 973 K, respectively [5,8]. This phenomenon has been attributed to the migration process from framework Fe^{3+} species to extraframework Fe^{2+} species. As the migration process in Fe-MCM-22 is less important than in Fe-silicalite (vide supra the EXAFS results), the observed red shift of the edge is of smaller entity.

Another interesting feature of the XANES spectra reported in Fig. 3 is the $1s \rightarrow 3d$ pre-edge peak (see inset for a magnified view) [4,5,8,67,68]. Position, intensity and shape are related to the oxidation state of iron and to its local geometry. From the XANES spectra of the model compounds, see Ref. [5] and Table 2, the $1s \rightarrow 3d$ pre-edge peak is observed at slightly higher energies for Fe^{3+} compounds (in the 7114.2–7114.6 eV) with respect to $FeCp_2$ (7112.5 eV). Moreover, its intensity is much higher for iron species in tetrahedral-like coordination as the $A_1 \rightarrow T_2$ transition is Laporte-allowed, while the $A_{1g} \rightarrow T_{2g}$ and $A_{1g} \rightarrow E_g$ transitions are symmetrically forbidden in the case of octahedral coordination. The spectrum of Fe-MCM-22 with template

Table 2
Position and normalized intensity of the $1s \rightarrow 3d$ pre-edge peak of the XANES spectra of Fe-MCM-22 after different treatments (Fig. 3). For comparison also data of different model compounds and of Fe-silicalite are repoted from Ref. [5]. (s) = shoulder. The edge of the $1s \rightarrow 3d$ peak of Fe metal foil (defined at the inflection point) has been set to 7111.6 eV

Sample	Pre-edge peak		Ref.
	Position (eV)	Intensity	
$FePO_4$	7114.2	0.133	[5]
Fe_2O_3	7113.4 (s)	0.056	[5]
	7114.6	0.080	
$Fe(acac)_3$	7113.5 (s)	0.048	[5]
	7114.6	0.053	
$FeCp_2$	7112.5	0.050	[5]
Fe-silicalite[a]	7114.2	0.205	[5]
Fe-silicalite[b]	7114.5	0.142	[5]
Fe-silicalite[c]	7111.8 (s)	0.037	[5]
	7114.5	0.128	
Fe-MCM-22[a]	7114.4	0.207	this work
Fe-MCM-22[b]	7114.3	0.151	this work
Fe-MCM-22[d]	7114.2	0.162	this work

[a] With template.
[b] Activated at 773 K.
[c] Activated at 973 K.
[d] After activation at 773 K and subsequent interaction with 15 Torr NO at RT.

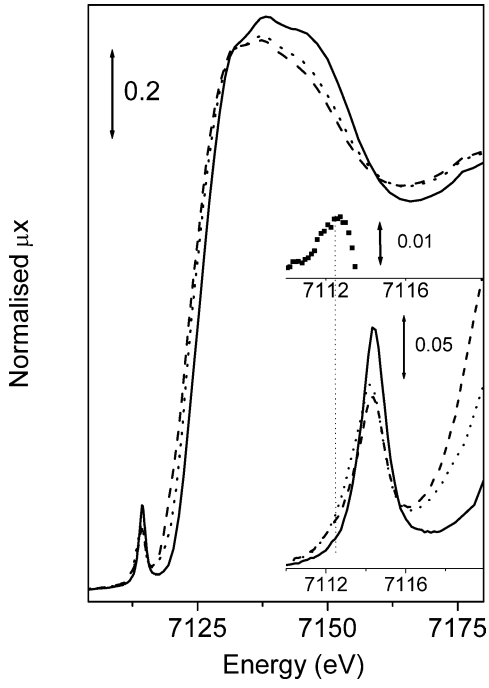

Fig. 3. XANES spectra of sample Fe-MCM-22 with template (solid line), after removal of template and subsequent activation at 773 K (dashed line) and subsequent adsorption of 15 NO at RT (dotted line). The inset shows the magnification of the pre-edge peaks. The scattered curve in the upper part of the inset is the difference between the spectrum of the activated sample and that of the sample with template. Vertical line indicates the position of the XANES band due to Fe^{2+} species, in $FeCp_2$, see Table 2.

(full line) exhibits the characteristic pre-edge peak of Fe^{3+} species in T_d-like symmetry: this holds for both peak position and intensity (compare with the data of $FePO_4$ and of Fe-silicalite with template, Table 2). The major change observed in the pre-edge peak upon calcination concerns the intensity reduction, revealing the decrease of iron framework species. The appearance of the XANES features of the extraframework species (about 30% according to the EXAFS signal) is hardly visible from the bare data (even in the inset) owing to the smaller extinction coefficient of the Laporte-forbidden electronic transition [5,8]. The high spectral resolution and the high S/N ratio of the XANES data here presented allows us to report a meaningful difference in XANES spectrum (calcined minus template, according to the established procedure used to present IR spectra) in the top part of the inset (scattered curve). From the difference in XANES spectrum a clear component at 7112.6 eV emerges. Comparison with the $FeCp_2$ model compound leads to the conclusion that we have singled out the XANES feature of the extraframework Fe^{2+} species.

As was the case in the EXAFS region of the X-ray absorption spectrum, also the XANES spectrum of the activated Fe-MCM-22 sample is not sensibly affected by NO dosage. We observe only a very small shift of the Fe K-edge towards higher energies (compare dashed and dotted curves in Fig. 3). When the same experiment is performed on a Fe-silicalite sample (unpublished results), a much larger edge shift is observed (more than 3 eV), which is interpreted as a significant electron donation from Fe^{2+} species to NO molecules. Comparing the XANES results of NO adsorption on Fe-silicalite (unpublished results), and on Fe-MCM-22 we conclude that in the MCM-22 case most of the iron atoms are not accessible to the probe molecule. This is well expected for the highly coordinated Fe^{3+} framework species but is rather surprising for the extraframework species which usually exhibits a high coordinative unsaturation [5,7,8,34,36]. This experimental evidence is tentatively explained in terms of a higher tendency to clustering of extraframework species in this sample with respect to the Fe-silicalite as investigated in Refs. [5,8]. It is difficult to say if the different topology and acidity of MCM-22 with respect to silicalite play an actual role in this different behavior, as for Fe-MCM-22 a much higher total amount of iron is concerned in the extraframework migration. In fact, in this case the migration concerns 30% out of 1/18 of T sites, resulting in $Fe_{extraframework}/Si = 1.67 \times 10^{-2}$, while for Fe-silicalite we were dealing with 58% out of 1/90 T sites resulting in $Fe_{extraframework}/Si = 6.4 \times 10^{-3}$.

3.3. IR spectroscopy of adsorbed NO

3.3.1. Band assignment

To gain further information on the oxidation and coordination state of extraframework species, IR spectroscopy of adsorbed NO has been applied. Nitric oxide is the suitable probe for this study due to its strong affinity towards Fe^{2+} and because of the high intensity of the ν_{NO} bands, as demonstrated by the abundant literature regarding Fe ions hosted in zeolitic matrix [5,7,34–36,38,39,48–50]. Accord-

ing to Refs. [5,7,34,36], the complex IR spectra obtained upon dosing NO on Fe containing zeolites has been interpreted on the basis of a pressure-dependent evolution from $Fe^{2+}(NO)$ and $Fe^{2+}(NO)_2$ complexes into $Fe^{2+}(NO)_3$ adducts. $Fe^{2+}(NO)$ complexes are characterised by a single N–O stretching mode around 1830 cm^{-1} while both $Fe^{2+}(NO)_2$ and $Fe^{2+}(NO)_3$ give rise to a doublet around 1840 and 1765 cm^{-1} (dinitrosyl) and 1916 and 1810 cm^{-1} (trinitrosyl). Such assignment was established also using a $^{15}NO/^{14}NO$ isotopic mixture [34] on Fe-silicalite samples characterised by remarkably well defined and narrow IR components [5,7,34,36]. Fig. 4 reports a high and a low NO coverage spectrum of a Fe-silicalite sample (Si/Fe = 90, Al free) for comparison.

The full-width at half maximum (FWHM) of the nitrosyl bands obtained upon dosing NO on Fe^{2+} species supported on siliceous matrices reflects the surface heterogeneity of the hosting sites for iron. On the basis of a systematic study of a large number of samples (differing on the support matrix and activation treatments) [5,7,8,34–36,38], we concluded that the surface heterogeneity of iron species could be explained by assuming the presence of $L_2N_nFe^{2+}$ centers, where L is a framework SiO^- (or atomic O^{2-}) chemically linked group and N is a framework oxygen atom of the vicinal SiOSi bridges electrostatically linked to iron. When zeolites are concerned, the value of n depends upon the location of the ions on the framework walls and defects. When probed with NO, the $L_2N_nFe^{2+}$ species are shown to be a composite family of sites, able to add either only three, two or one NO ligands, i.e.: L_2NFe^{2+}, $L_2N_2Fe^{2+}$ and $L_2N_3Fe^{2+}$. On this basis, the formation of the mono-, di- and trinitrosyl species can be described as follows:

$$L_2N_jFe^{2+} \xrightarrow{NO} L_2N_jFe^{2+}(NO), \quad (1)$$

$$L_2N_kFe^{2+} \xrightarrow{2NO} L_2N_kFe^{2+}(NO)_2 \overset{NO}{\rightleftharpoons} L_2N_kFe^{2+}(NO)_3, \quad (2)$$

where the addition of NO occurs on structurally different sites and where the number of adsorbed NO is greater on the most coordinatively unsaturated sites ($k < j$). This model was able to explain the whole set of spectroscopic data collected so far.

This holds also for the experiment performed on Fe-MCM-22 and reported in Fig. 5a. By comparison with the spectra reported in Fig. 4, besides the higher FWHM of all components, it can be observed that the NO bands obtained on Fe-MCM-22 are qualitatively similar to those obtained on Fe-silicalite, indicating that also in this case extraframework Fe^{2+} species are formed. The conversion of the pair of bands at 1912 and 1812 cm^{-1} into the 1835 (shoulder) and 1764 cm^{-1} pair upon evacuating NO is observed. According to the Fe-silicalite case [5], these spectroscopic manifestations have been assigned to the right-hand equilibrium in reaction (2). The $L_2N_kFe^{2+}(NO)_2$ complexes are responsible for the pair of bands at 1835 (shoulder) and 1764 cm^{-1}, while $L_2N_kFe^{2+}(NO)_3$ generate the bands at 1912 and 1812 cm^{-1}. As already observed in Fe-silicalite, beside the di- and trinitrosyl complexes, a third species is responsible for the component at around 1830 cm^{-1}, assigned to a $L_2N_jFe^{2+}(NO)$ complex ($j = 3$). In the Fe-MCM-22 sample studied in this work the concentration of this complex is higher indicating that, on an average, extraframework Fe species exhibit a lower coordinative unsaturation with respect to Fe-silicalite.

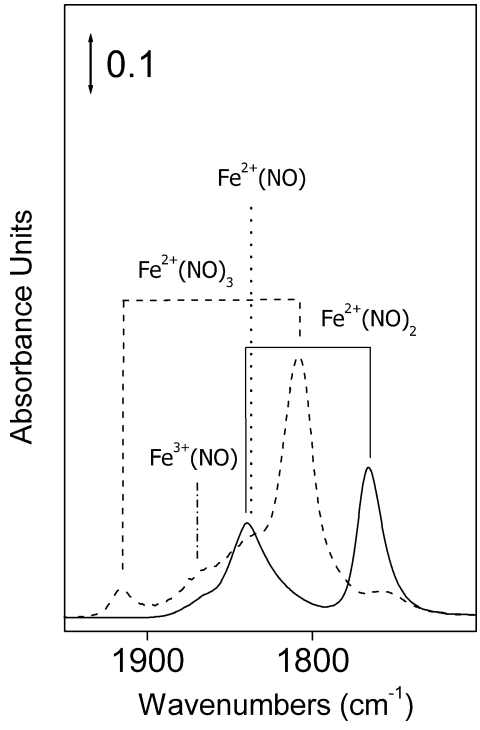

Fig. 4. IR spectra of NO dosed at RT on Fe-silicalite sample (Si/Fe = 90, Al free) at low (solid spectrum) and high (dashed spectrum) equilibrium pressures.

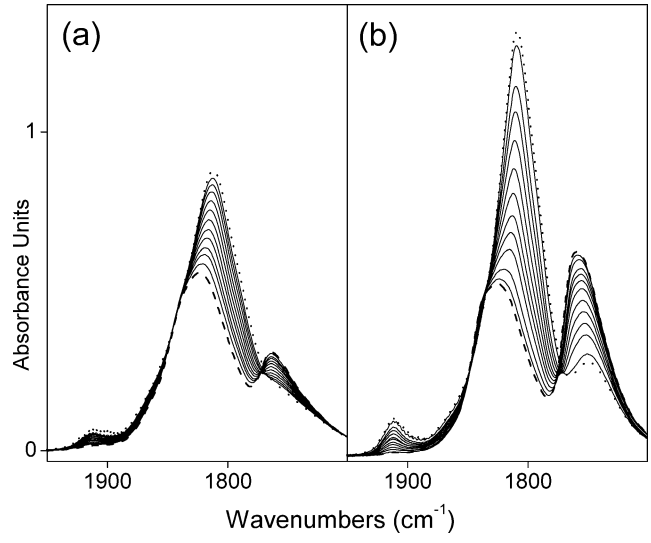

Fig. 5. Room temperature IR spectra of increasing P_{NO} (from dashed to dotted curves) dosed on Fe-MCM-22 activated at 773 K, prior to (part a) and after (part b) preadsorption of water.

According to what is found in the studies devoted to Fe-silicalite samples, the $L_2N_nFe^{2+}$ species detected by NO adsorption are families of sites with slightly different local environment depending on the ion location in the matrix inner voids. In the case of the Fe-MCM-22 studied in this work, the nitrosyl bands are strongly asymmetric and very broad, indicating that the families of $L_2N_nFe^{2+}$ species exhibits a higher heterogeneity with respect of that formed in Fe-silicalite. By comparing the IR spectra reported here with those obtained on Fe-silicalite [5,7,34] (see also Fig. 4) and with those obtained by Dumesic and coworkers [69,70] and by Berlier et al. [38] on amorphous Fe/SiO_2 samples, we can conclude that the heterogeneity of extraframework Fe^{2+} hosted in MCM-22 is intermediate. The small differences in the position of the maxima can be explained in terms of the variability in the families of sites formed in the different matrix: such as distribution of framework Al^{3+} species in the surrounding [7].

3.3.2. *Effect of water preadsorption*

In Fig. 5b, spectra obtained upon adsorption of NO on the same Fe-MCM-22 sample previously contacted with water vapor are reported. By comparison with the spectra obtained prior to water adsorption (Fig. 5a), the following comments can be done. After water dosage, the bands at 1912, 1812 and 1764 cm^{-1} are more intense and narrow (FWHM moving from 57 to 40 cm^{-1}). As far as the intensities are concerned, we observe a clear increase of both trinitrosyl modes and of the low frequency mode of the dinitrosyl complexes (see Fig. 4 for assignments). Conversely, the adsorption around 1830 cm^{-1}, including both the mononitrosyl mode and the high frequency mode of the dinitrosyl adduct, seems to be almost unaffected (only a slight decrease is observed).

In the Fe-silicalite case [5,34], the lower Fe heterogeneity allowed us to clearly observe that pretreatment with H_2O vapor caused the decrease of the mononitrosyl band accompanied by the parallel increase of the four components of di- and trinitrosyl species. In the present case, the apparent invariance of the absorption around 1830 cm^{-1} is likely due to the much broader character of all spectroscopic features. The same interpretation can thus hold also in the Fe-MCM-22 case: water preadsorption causes the decrease of $L_2N_jFe^{2+}(NO)$ complex in favor of the parallel increase of $L_2N_kFe^{2+}(NO)_3$ and $L_2N_kFe^{2+}(NO)_2$ complexes ($k < j$), see reactions (1) and (2). On an atomistic level, these spectroscopic observations can be rationalized in terms of the extraction of Fe^{2+} by water from the original coordination sphere, favoring the multiple addition of strong ligands such NO [5,34] according to the scheme:

$$L_2N_jFe^{2+} \overset{n\mathrm{H_2O}}{\rightarrow} L_2N_kFe^{2+}(H_2O)_n \overset{m\mathrm{NO}}{\rightleftharpoons} L_2N_kFe^{2+}(NO)_m + n\mathrm{H_2O}, \quad (3)$$

where $k < j$, $m = 2$ or 3. This phenomenon is not observed when probe molecules having a lower affinity toward Fe^{2+} are used, such as CO or N_2O [5]. We can therefore conclude that the spectra reported in Fig. 5b can be explained with a ligand displacement reaction [71] where H_2O extracts the Fe^{2+} ions from the original coordination sphere, substituting the weak "*N*" ligands. NO, thanks to its high affinity for Fe^{2+} species, is able to displace water ligands forming $L_2N_kFe^{2+}(NO)_2$ and $L_2N_kFe^{2+}(NO)_3$ complexes. This effect also causes a decrease in the heterogeneity of the Fe^{2+} family, resulting in the narrowing of the bands.

As a further observation, we report that adsorption of water on preadsorbed NO causes a significant decrease of the mononitrosyl adducts, while the poli-nitrosyl ones are almost unaffected (experiment not reported, for brevity). Note that a similar behavior was observed for the Fe-silicalite system too [5].

The ability of "water treated" iron species to form nitrosyl complexes with higher nuclearity does not directly imply an increased activity. In fact, after interaction with water, Fe species did not exhibit an average lower coordination state but have just replaced *N* surface ligand with H_2O ligands. We expect an increased catalytic activity only if the reactants are able to displace water. This is not the case for N_2O, as probed by IR spectra of N_2O dosed on Fe-silicalite prior to and after contact with water, parts (a) and (b) of Fig. 6, respectively. On the activated sample (Fig. 6a), the adsorption of N_2O generates three bands at 2275, 2235, and 2218 cm^{-1}. The first two are attributed to N_2O adsorbed on Fe^{3+} and Fe^{2+} centres, respectively. The strong and narrow band at 2218 cm^{-1} (with a shoulder at 2200 cm^{-1}) is due to physically adsorbed N_2O and is the only one present on silicalite (dotted line in Fig. 6). For a more detailed assignment of these spectra the readers are referred to Ref. [5]. For the time being, it is just relevant to observe that after water preadsorption almost all the spectroscopic features ascribed to N_2O interacting with extraframework iron species are ab-

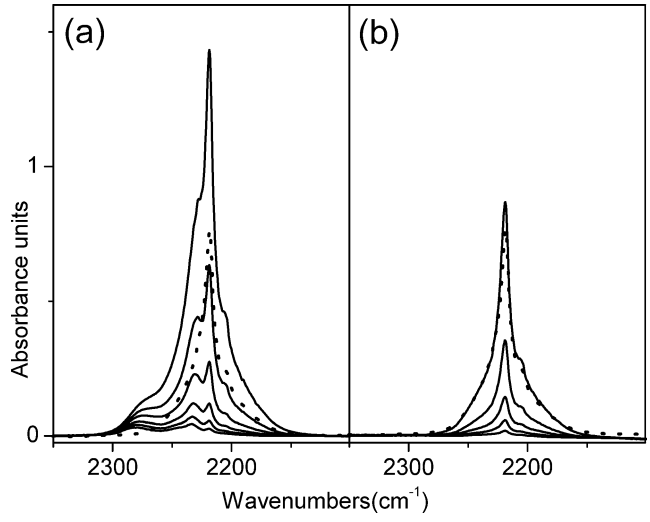

Fig. 6. Room temperature IR spectra of increasing pressures of N_2O, up to 30 Torr, dosed on Fe-silicalite (Si/Fe = 90, Al free) activated at 973 K, prior to (part a) and after (part b) preadsorption of water. The dotted spectrum reported in both parts was obtained upon adsorption of N_2O (30 Torr) on a defective silicalite (Fe and Al-free).

sent. The spectrum obtained at the higher pressure is very close to that obtained on the Fe and Al-free zeolite with the same topology. This implies that N_2O is not able to displace water ligands and explains why literature data reports a decrease of the catalytic activity in the N_2O decomposition of Fe-zeolites previously contacted with water [72–74].

3.3.3. Effect of red–ox treatments

After interaction with O_2 at 573 K, the catalyst shows a markedly modified affinity towards NO adsorption, reflecting a deep modification of the extraframework iron sites (compare Figs. 5a and 7a). In fact, a dramatic depression of all ferrous nitrosyl complexes is observed. At the same time, new weak bands are formed in the 2125–2000 cm^{-1} interval (inset). Similar adsorptions were observed by directly dosing NO_2 on the sample (not reported here for brevity, see e.g. the spectra reported in Ref. [75] for comparison) indicating that oxidation products are formed. These observations imply that the oxidation treatment causes the formation of adsorbed oxygen on the extraframework iron centers. It is not possible from these results to infer the structure of the adsorbed species. The only conclusion is that adsorbed oxygen coming from O_2 shields efficiently the Fe centers and it is not rapidly nor completely removed by NO at RT. In fact, only a small quantity of adsorbed oxygen reacts with NO to give adsorbed NO_2 species.

The effect of reduction with H_2 is reported in Fig. 7b. In this case the nitrosyl bands formed on the sample are very similar to those obtained before red–ox treatments except for a small increase in the overall intensity. This implies that after the reductive treatment, the concentration of the Fe^{2+} species accessible to the interaction with NO has increased. We can hypothesize that these new species are produced upon reduction of extraframework Fe^{3+} species. In Fe-silicalite samples, the formation of Fe^{3+}(NO) adducts

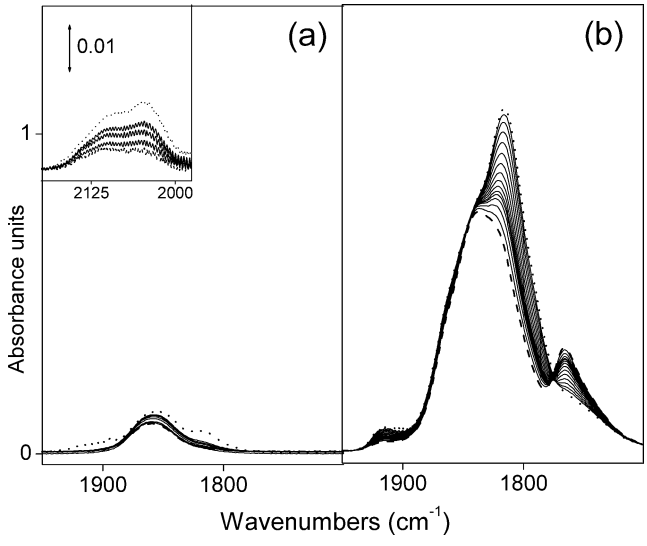

Fig. 7. Room temperature IR spectra of increasing P_{NO} (from dashed to dotted curves) dosed on Fe-MCM-22 activated at 773 K, after oxidation in O_2 at 573 K (part a) and after subsequent reduction in H_2 at 573 K (part b).

adsorbing around 1865 cm^{-1} (see Fig. 4) was observed. In the present case, a similar adsorption was not observed in any of the experiments. However, since these complexes are characterised by a low IR intensity, they were probably shadowed by the broad bands due to Fe^{2+}(NO) complexes.

4. Conclusions

An isomorphously substituted Fe-MCM-22 sample with high iron content (Si/Fe = 18) was characterised by FTIR, EXAFS and XANES spectroscopies. Comparisons with the Fe-silicalite system are made. Before template burning isolated Fe^{3+} species are found in well-defined tetrahedral-like geometry. Upon template burning and subsequent activation in vacuo, a fraction of framework Fe^{3+} species migrates to extraframework positions, forming a mixture of Fe^{2+} and Fe^{3+} ions. The Fe^{2+} sites represent the majority of extraframework species, and form, upon NO contact, stable $Fe^{2+}(NO)_n$ complexes ($n = 1, 2, 3$). Due to the broad and asymmetric character of the corresponding IR bands, the formation of Fe^{3+}(NO) complexes could not be clearly detected. The broadness of the IR bands testifies a high heterogeneity of extraframework sites, and the presence of small oxidic clusters. The latter observation is in agreement with XANES results. If the large clustering process is related to the topology and acidity of MCM-22 structure is hard to say, due to the large iron content of the sample.

Upon water preadsorption, the nature and distribution of extraframework species is influenced. In particular, Fe^{2+}(NO) species become able to adsorb more NO molecules, forming $Fe^{2+}(NO)_3$ complexes. This phenomenon was explained with a ligand displacement reaction. Upon oxidation (with O_2 at 573 K) adsorbed oxygen is formed, which efficiently shields the Fe centers and does not rapidly nor efficiently react with NO. Upon reduction, the intensity of nitrosyl complexes increases, indicating the reduction of extraframework Fe^{3+} (likely present on the surface of small oxidic clusters) to Fe^{2+}.

Acknowledgments

We are indebted with R. Aiello and F. Testa for sample synthesis and fruitful discussion. We thank F. D'Acapito and all the GILDA BM8 staff at the ESRF, where X-ray absorption measurements have been carried out and C. Prestipino for precious help in the EXAFS analysis.

References

[1] G.T. Kokotailo, S.L. Lawton, G.T. Olson, W.M. Meier, Nature 272 (1978) 437.
[2] S.A. Axon, K. Huddersman, J. Klinowski, Chem. Phys. Lett. 172 (1990) 398.
[3] R. Szostak, T.L. Thomas, J. Catal. 100 (1986) 555.

[4] S. Bordiga, R. Buzzoni, F. Geobaldo, C. Lamberti, E. Giamello, A. Zecchina, G. Leofanti, G. Petrini, G. Tozzola, G. Vlaic, J. Catal. 158 (1996) 486.
[5] G. Berlier, G. Spoto, S. Bordiga, G. Ricchiardi, P. Fisicaro, A. Zecchina, I. Rossetti, E. Selli, L. Forni, E. Giamello, C. Lamberti, J. Catal. 208 (2002) 64.
[6] C. Lamberti, G. Turnes Palomino, S. Bordiga, D. Arduino, A. Zecchina, G. Vlaic, Jpn. J. Appl. Phys. 38–1 (1999) 55.
[7] G. Berlier, A. Zecchina, G. Spoto, G. Ricchiardi, S. Bordiga, C. Lamberti, J. Catal. 215 (2003) 264.
[8] G. Berlier, G. Spoto, P. Fisicaro, S. Bordiga, A. Zecchina, E. Giamello, C. Lamberti, Microchem. J. 71 (2002) 101.
[9] A. Zecchina, S. Bordiga, G. Spoto, D. Scarano, G. Petrini, G. Leofanti, M. Padovan, C. Otero Areán, J. Chem. Soc. Faraday Trans. 88 (1992) 2959.
[10] A. Zecchina, F. Geobaldo, C. Lamberti, S. Bordiga, G. Turnes Palomino, C. Otero Areán, Catal. Lett. 42 (1996) 25.
[11] Y. Ono, K. Kanae, J. Chem. Soc. Faraday Trans. 87 (1991) 669.
[12] C.R. Bayense, A.J.M.P. van der Pal, J.H.C. van Hooff, Appl. Catal. 72 (1991) 81.
[13] B.S. Kwak, W.M.H. Sachtler, J. Catal. 145 (1994) 456.
[14] A.S. Kharitonov, G.A. Sheveleva, G.I. Panov, V.I. Sobolev, Y.A. Paukshtis, V.N. Romannikov, Appl. Catal. A 98 (1993) 33.
[15] D. Meloni, R. Monaci, V. Solinas, G. Berlier, S. Bordiga, I. Rossetti, C. Oliva, L. Forni, J. Catal. 214 (2003) 169.
[16] K. Weissermehl, H.J. Arpe, Industrial Organic Chemistry, VCH, New York, 1993, p. 344.
[17] X. Feng, W.K. Hall, J. Catal. 166 (1997) 368.
[18] H.Y. Chen, X. Wang, W.M.H. Sachtler, Phys. Chem. Chem. Phys. 2 (2000) 3083.
[19] A.A. Battiston, J.H. Bitter, D.C. Kroningsberger, J. Catal. 218 (2003) 163.
[20] R. Brosius, D. Habermacher, J.A. Martens, L. Vradman, M. Herskowitz, L. Capek, Z. Sobalik, J. Dedecek, B. Wichterlova, V. Tokarova, O. Gonsiorova, Top. Catal. 30–31 (2004) 333.
[21] E.J.M. Hensen, Q. Zhu, M.M.R.M. Hendrix, A.R. Overweg, P.J. Kooyman, M.V. Sychev, R.A. van Santen, J. Catal. 221 (2004) 560.
[22] P. Marturano, A. Kogelbauer, P. Prins, J. Catal. 190 (2000) 460.
[23] P. Marturano, L. Drozdova, A. Kogelbauer, R. Prins, J. Catal. 192 (2000) 236.
[24] P. Marturano, L. Drozdova, G.D. Pirngruber, A. Kogelbauer, R. Prins, Phys. Chem. Chem. Phys. 3 (2001) 5585.
[25] G.D. Pirngruber, J. Catal. 219 (2003) 456.
[26] E.J.M. Hensen, Q. Zhu, M.M.R.M. Hendrix, A.R. Overweg, P.J. Kooyman, M.V. Sychev, R.A. van Santen, J. Catal. 221 (2004) 560.
[27] Q. Zhu, R.M. van Teeffelen, R.A. van Santen, E.J.M. Hensem, J. Catal. 221 (2004) 575.
[28] A. Meagher, V. Nair, R. Szostak, Zeolites 8 (1988) 3.
[29] P. Fejes, K. Lazar, I. Marsi, A. Rockenbauer, L. Korecz, J.B. Nagy, S. Perathoner, G. Centi, Appl. Catal. A 252 (2003) 75.
[30] A. Ribera, I.W.C.E. Arends, S. de Vries, J. Pérez-Ramírez, R.A. Sheldon, J. Catal. 195 (2000) 287.
[31] V.I. Sobolev, G.I. Panov, A.S. Kharitonov, V.N. Romannikov, A.M. Volodin, K.G. Ione, J. Catal. 139 (1993) 435.
[32] S.A. Axon, K.K. Fox, S.W. Carr, J. Klinowski, Chem. Phys. Lett. 189 (1992) 1.
[33] D.W. Lewis, R.A. Catlow, J. Sankar, S.W. Carr, J. Phys. Chem. 99 (1995) 2377.
[34] G. Spoto, A. Zecchina, G. Berlier, S. Bordiga, M.G. Clerici, L. Basini, J. Mol. Catal. A 158 (2000) 107.
[35] A.M. Ferretti, C. Oliva, L. Forni, G. Berlier, A. Zecchina, C. Lamberti, J. Catal. 208 (2002) 83.
[36] G. Berlier, G. Spoto, G. Ricchiardi, S. Bordiga, C. Lamberti, A. Zecchina, J. Mol. Catal. A 182–183 (2002) 359.
[37] C. Nozaki, C.G. Lugmair, A.T. Bell, T.D. Tilley, J. Am. Chem. Soc. 124 (2002) 13194.
[38] G. Berlier, F. Bonino, A. Zecchina, S. Bordiga, C. Lamberti, Chem Phys Chem. 4 (2003) 1073.
[39] G. Mul, M.W. Zandbergen, F. Kapteijn, J.A. Moulijn, J. Perez-Ramirez, Catal. Lett. 93 (2004) 113.
[40] P. Wu, H. Lin, T. Komatsu, T. Yashima, Chem. Commun. (1997) 663.
[41] F. Testa, F. Crea, G.D. Diodati, L. Pasqua, R. Aiello, P. Lentz, J.B. Nagy, Micropor. Mesopor. Mater. 30 (1999) 187.
[42] D. Meloni, R. Monaci, E. Rombi, C. Guimon, H. Martinez, I. Fechete, E. Dumitriu, Stud. Surf. Sci. Catal. 142 (2002) 167.
[43] M.E. Leonowicz, J.A. Lawton, S.L. Lawton, M.K. Rubin, Science 264 (1994) 1910.
[44] A. Corma, C. Corell, J. Pèrez-Patiente, Zeolites 15 (1995) 2.
[45] W. Souverijns, W. Verrelst, G. Vanbutsele, J.A. Martens, P.A. Jacobs, J. Chem. Soc., Chem. Commun. (1994) 1671.
[46] G.J. Kennedy, S.L. Lawton, M.K. Rubin, J. Am. Chem. Soc. 116 (1994) 11000.
[47] S.L. Lawton, M.E. Leonowicz, R.D. Partridge, P. Chu, M.K. Rubin, Micropor. Mesopor. Mat. 23 (1998) 109.
[48] L.J. Lobree, I.C. Hwang, J.A. Reimer, A.T. Bell, J. Catal. 186 (1999) 242.
[49] H.-Y. Chen, El-M. El-Malki, X. Wang, R.A. van Santen, W.M.H. Sachtler, J. Mol. Catal. A 162 (2000) 159.
[50] G. Mul, J. Perez-Ramirez, F. Kapteijn, J.A. Moulijn, Catal. Lett. 80 (2002) 129.
[51] B.R. Wood, J.A. Reimer, A.T. Bell, M.T. Janicke, K.C. Ott, J. Catal. 224 (2004) 148.
[52] S.H. Choi, B.R. Wood, A.T. Bell, M.T. Janicke, K.C. Ott, J. Phys. Chem. B 108 (2004) 8970.
[53] S.H. Choi, B.R. Wood, J.A. Ryder, A.T. Bell, J. Phys. Chem. B 107 (2003) 11843.
[54] G.D. Pirngruber, M. Luechinger, P.K. Roy, A. Cecchetto, P. Smirniotis, J. Catal. 224 (2004) 429.
[55] S. Pascarelli, F. Boscherini, F. D'Acapito, C. Meneghini, J. Hrdy, S. Mobilio, J. Synchrotron Rad. 3 (1996) 147.
[56] C. Lamberti, S. Bordiga, F. Bonino, C. Prestipino, G. Berlier, L. Capello, F. D'Acapito, F.X. Llabrés i Xamena, A. Zecchina, Phys. Chem. Chem. Phys. 5 (2003) 4502.
[57] C. Lamberti, C. Prestipino, S. Bordiga, G. Berlier, G. Spoto, A. Zecchina, A. Laloni, F. La Manna, F. Danca, R. Felici, F. D'Acapito, P. Roy, Nucl. Instr. Meth. B 200 (2003) 196.
[58] C. Lamberti, S. Bordiga, A. Zecchina, M. Salvalaggio, F. Geobaldo, C. Otero Areán, J. Chem. Soc. Faraday Trans. 94 (1998) 1519.
[59] P. Wu, T. Komatsu, T. Yashima, Micropor. Mesopor. Mater. 22 (1998) 343.
[60] M. De Crescenci, A. Balzarotti, F. Comin, L. Incoccia, S. Mobilio, N. Motta, Solid State Commun. 37 (1981) 921.
[61] E.C. Marques, D.R. Sandstrom, F.W. Lytle, R.B. Greegor, J. Chem. Phys. 77 (1982) 1027.
[62] C. Lamberti, G. Turnes Palomino, S. Bordiga, A. Zecchina, G. Spano, C. Otero Areán, Catal. Lett. 63 (1999) 213.
[63] A. Bianconi, in: D.C. Koningsberger, R. Prins (Eds.), X-Ray Absorption, Willey, New York, 1988, p. 573.
[64] C. Lamberti, G. Turnes Palomino, S. Bordiga, G. Berlier, F. D'Acapito, A. Zecchina, Angew. Chem. Int. Ed. 39 (2000) 2138.
[65] C. Lamberti, C. Prestipino, F. Bonino, L. Capello, S. Bordiga, G. Spoto, A. Zecchina, S. Diaz Moreno, B. Cremaschi, M. Garilli, A. Marsella, D. Carmello, S. Vidotto, G. Leofanti, Angew. Chem. Int. Ed. 41 (2002) 2341.
[66] T.E. Westre, P. Kennepohl, J.G. DeWitt, B. Hedman, K.O. Hodgson, E.I. Solomon, J. Am. Chem. Soc. 119 (1997) 6297.
[67] A. Manceau, A.I. Gorshkov, V.A. Dirits, Am. Mineralogist 77 (1992) 1133.

[68] K. Lawniczak-Jablonska, J.R. Iawanowski, Z. Golacki, A. Traverse, S. Pizzini, A. Fotaine, I. Winter, J. Hormes, Phys. Rev. B 53 (1996) 1119.
[69] S. Yuen, Y. Chen, J.E. Kubsh, J.A. Dumesic, N. Topsøe, H. Topsøe, J. Phys. Chem. 86 (1982) 3022.
[70] D.G. Rethwisch, J.A. Dumesic, J. Phys. Chem. 90 (1986) 1625.
[71] D.S. Bohle, C.-H. Hung, J. Am. Chem. Soc. 117 (1995) 9584.
[72] L. Kiwi-Minsker, D.A. Bulushev, A. Renken, Catal. Today 91–92 (2004) 165.
[73] L. Kiwi-Minsker, D.A. Bulushev, A. Renken, J. Catal. 219 (2003) 273.
[74] L. Kiwi-Minsker, D.A. Bulushev, A. Renken, J. Catal. 222 (2004) 389.
[75] J. Szanyi, J.H. Kwak, C.H.F. Peden, J. Phys. Chem. B 108 (2004) 3746.